Figure S1

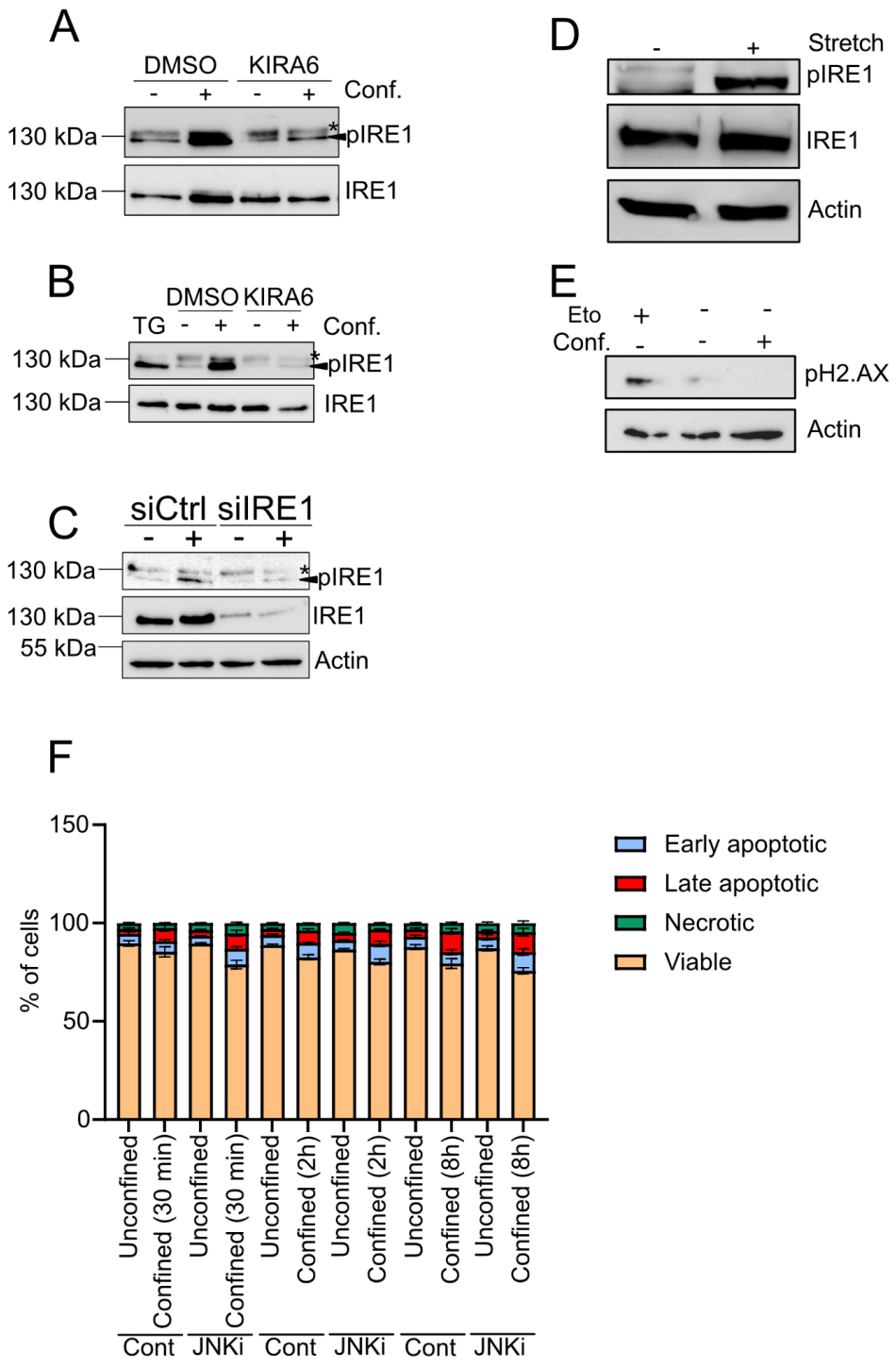

Figure S1: ***A:*** HeLa cells were treated with DMSO or 1 µM of KIRA6 for 1 h and then either left undisturbed (-) or exposed to 3 µm confinement (+) for 30 min, followed by lysis and immunoblotting as indicated. The asterisk marks the unspecific band and the arrowhead points to phospho-IRE1. ***B:*** HeLa cells were treated with 3 µM of thapsigargin (TG) for 1 h or incubated with DMSO or 1 µM of KIRA6 for 1 h and then either left undisturbed (-) or exposed to 3 µm confinement (+) for 30 min, followed by lysis and immunoblotting as indicated. The asterisk marks the unspecific band and the arrowhead points to phospho-IRE1. ***C:*** HeLa cells were transfected with non-targeting siRNA (siCtrl) or siRNA against IRE1 (siIRE1). After 72 h, both siCtrl and siIRE1 treated cells were either confined

to 3 µm for 30 min or left undisturbed for the same time period, followed by lysis and immunoblotting as indicated. The asterisk marks the unspecific band and the arrowhead points to phospho-IRE1. ***D:*** HeLa cells were either left undisturbed (-) or exposed to uniaxial stretching of maximally 50% for 30 min (+), followed by lysis and immunoblotting as indicated. ***E:*** HeLa cells were treated with 5 µM of Etoposide (Eto) for 6 h, left undisturbed (-) or exposed to confinement to 3 µm for 30 min (+) followed by lysis and immunoblotting. ***F:*** HeLa cells were treated with a JNK inhibitor (SP600125, 10 µM) or with DMSO as a solvent control. Then, cells were left undisturbed or exposed to 3 µm confinement for the indicated duration. Cells were collected and apoptosis measured by flow cytometry analysis using Annexin V and Propidium Iodide apoptosis detection kit according to the manufacturer's protocols. Quantifications of all immunoblots are available in supplementary Table S2.

Figure S2

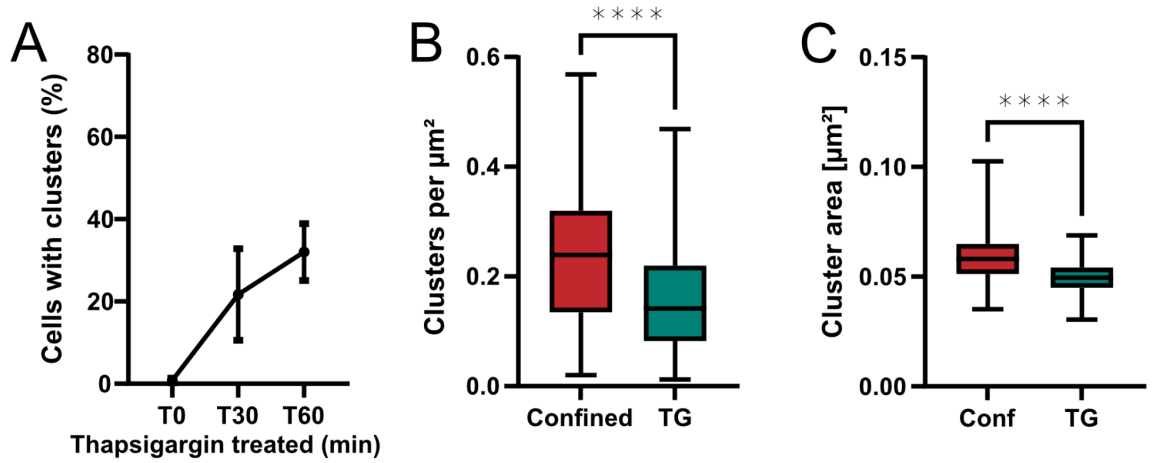

Figure S2. ***A-C:*** HeLa cells expressing GFP-tagged wild-type IRE1 were treated with 3 µM thapsigargin (TG) for the indicated duration. Cells were imaged at 1-5 min intervals. Cells with clusters were counted manually. Error bars represent SD from two experiments (A). The number of clusters per cell as well as the density of clusters per cell (B) and the average cluster area (C) were determined using Fiji. "Confined" indicates cells that were subjected to 3 µm confinement for 60 minutes.

Figure S3

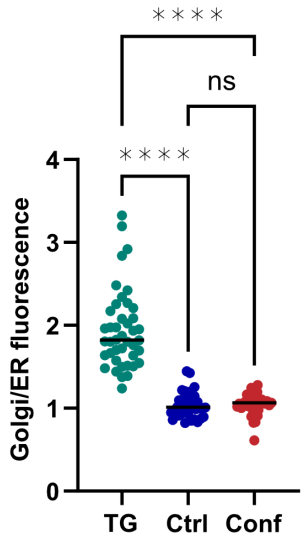

Figure S3. ***A:*** Confinement does not induce ATF6 activation. HeLa cells were transfected with an ATF6 activity reporter. The reporter consists of a GFP-tagged mutant version of ATF6 (R415A/R416A), which is resistant to proteolytic cleavage in the Golgi apparatus. Upon induction of the UPR, the reporter accumulates at the Golgi and the extent of Golgi fluorescence normalized to the ER is a reflection of ATF6 activation. 24 h after transfection, cells were treated with 3 µM of thapsigargin (TG) for 3 hours, or subjected to 3 µm confinement for 1 h, or left undisturbed, followed by fixation and immunofluorescence staining for GM130. Golgi and ER fluorescence intensities were measured in Fiji. p-values were calculated using ordinary one-way ANOVA followed by Tukey's multiple comparisons test (ns $p>0.05$, ****$p<<0.001$).

Figure S4

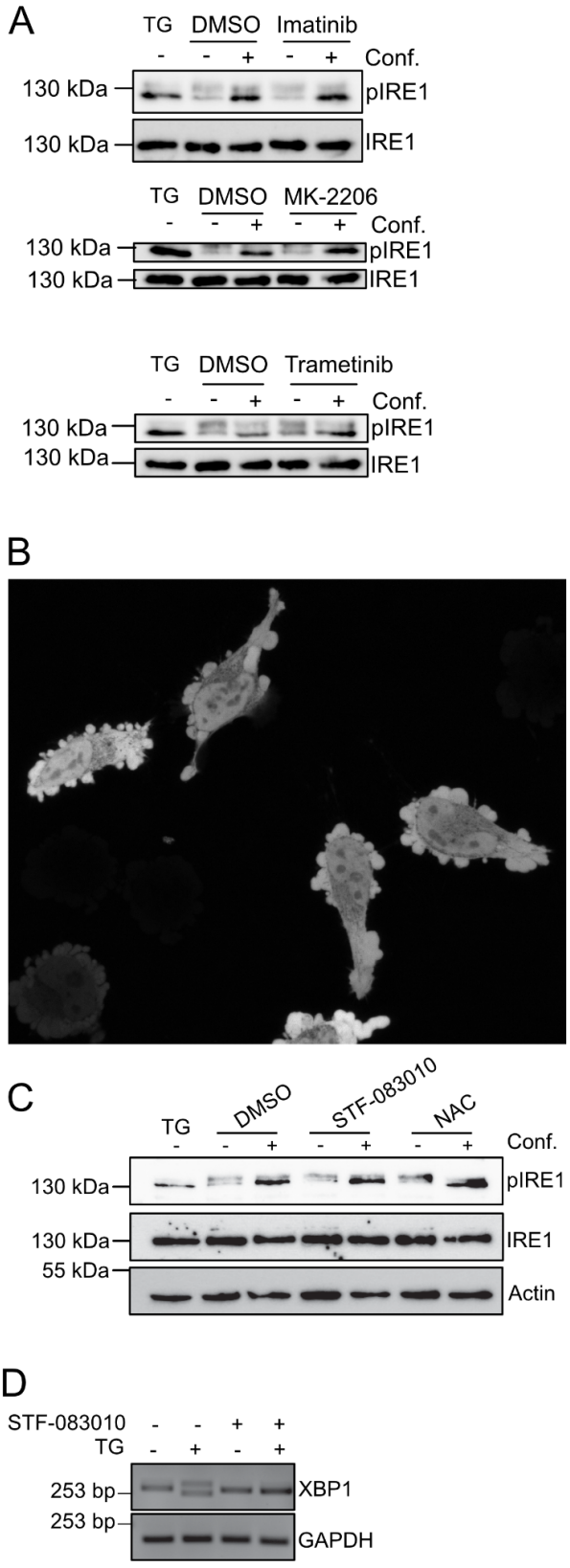

Figure S4. ***A:*** HeLa cells were pre-treated with DMSO, the cAbl inhibitor imatinib (Imat, 10 µM, 2 h pre-incubation before confinement), the MEK1/2 inhibitor trametinib (Tram, 100 nM, 1 h pre-incubation), or the Akt inhibitor MK-2206 (1 µM, 3 h pre-incubation). Cells were either not confined (-) or confined to 3 µm (+) for 30 min followed by lysis and immunoblotting as indicated. ***B:*** HeLa

expressing GFP were confined to 3 μm and imaged using fluorescence microscopy. ***C*****:** HeLa cells were pre-treated with solvent (DMSO), the IRE1 RNase domain inhibitor STF-083010 (40 μM, 1 h pre-incubation before confinement), or N-acetyl cysteine (NAC) (5 μM, 2 h pre-incubation before confinement). Cells were either not confined (-) or confined to 3 μm (+) for 30 min followed by lysis and immunoblotting as indicated. TG indicates treatment with thapsigargin. ***D:*** HeLa cells were pre-treated with DMSO or 40 μM of STF083010 for 30 min, followed by treatment with DMSO or 3 μM of thapsigargin (TG) for 2 h, followed by RNA extraction and PCR for XBP1 and GAPDH. Samples were run on a 3% agarose gel. Immunoblots in panel A are representative of 3 independent experiments. Immunoblot in panel C is representative of 2 independent experiments. Quantifications of all immunoblots are available in supplementary Table S2.

Figure S5

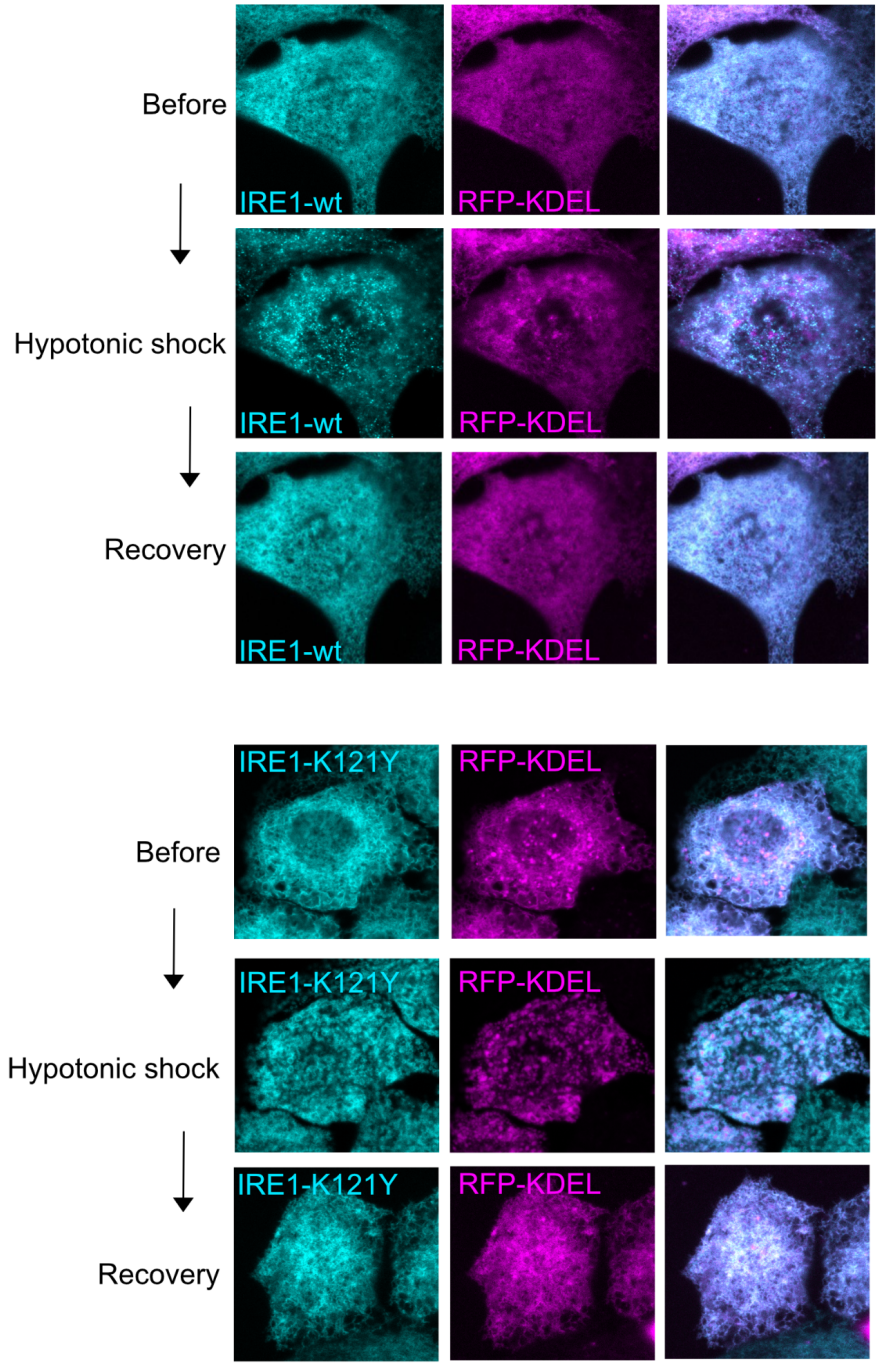

Figure S5. Single channel images of the cells shown in Figure 3A-B.

Figure S6

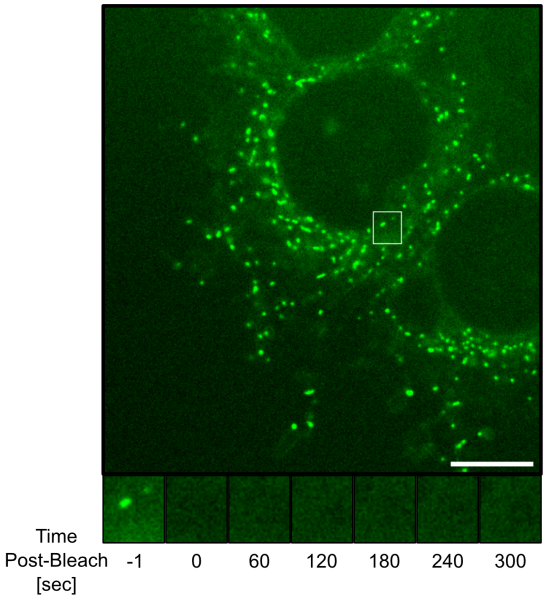

Figure S6. HeLa cells expressing GFP-tagged wild type IRE1 were subjected to confinement 3 μm for 1 h. After formation of clusters, FRAP assays were conducted, by bleaching individual clusters and monitoring their recovery. Image shows a representative example where an IRE1 cluster was bleached and the recovery of fluorescence was detected up to 300 seconds after bleaching. Scale bar 10 μm.

Figure S7

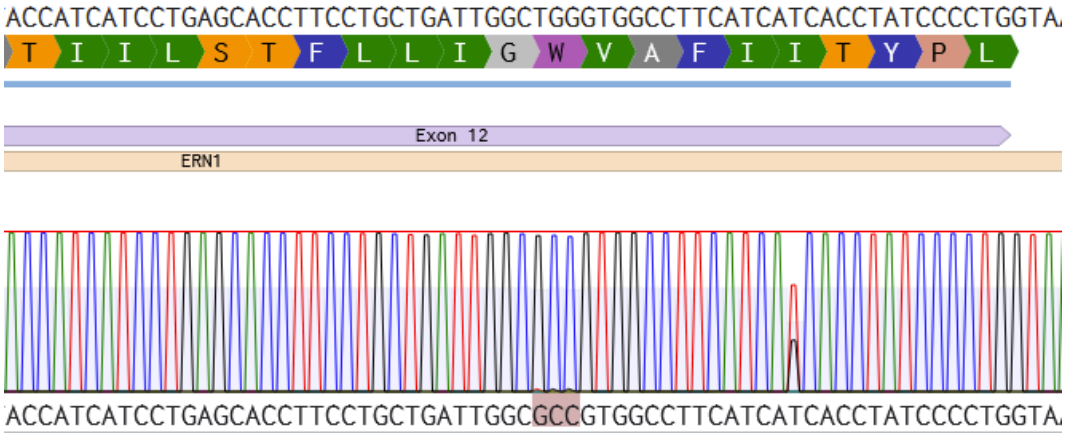

Figure S7. Validation of IRE1 W457A genome editing. Amplicon-based nanopore sequencing of *ERN1* exon 12 confirmed replacement of the wild-type tryptophan 457 codon (TGG) with an alanine codon (GCC) in the HEK293A clone used for experiments shown in Figures 4C, 5C, and S8. All detected *ERN1* alleles carried the W457A edit, while one of three alleles additionally contained an I462S substitution (ATC→AGC).

Figure S8

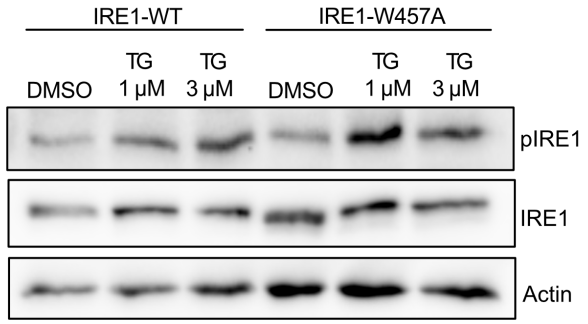

Figure S8. HEK293A IRE1-W457A cells are able to sense proteotoxic stress. Wild-type HEK293A (WT) or cells with gene-edited IRE1-W457A were treated with 1 µM or 3 µM thapsigargin (TG) for 1 h, lysed, and immunoblotted as indicated. Quantifications of all immunoblots are available in supplementary Table S2.

Figure S9

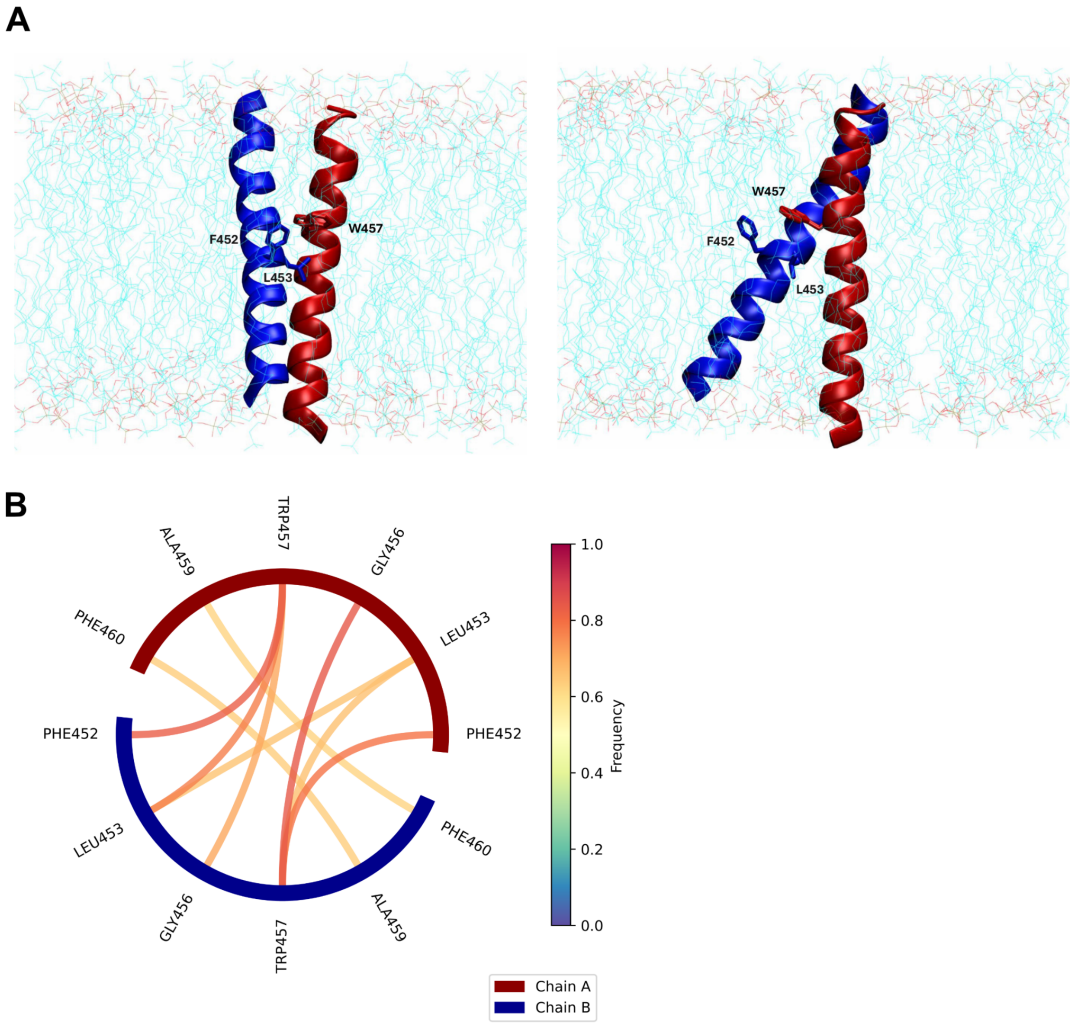

Figure S9. Role of W457 in IRE1 dimerization. ***A:*** Orthogonal views of the AlphaFold3 model for the IRE1 homodimer embedded in the lipid bilayer used in the Molecular Dynamics simulations. The lipids are shown in lines and colored by atom name. Sidechains of W457, and its main interaction partners F452 and L453, are shown in licorice. ***B:*** Flareplot of the interactions between the IRE1 monomers during 30 µs long Molecular Dynamics simulations. Chain A (helix 1) is shown in red and chain B (helix 2) is shown in blue. The interaction lines are colored according to the contact frequency during the simulations. Only interactions with mean contact frequency above 0.6 are shown.

Figure S10

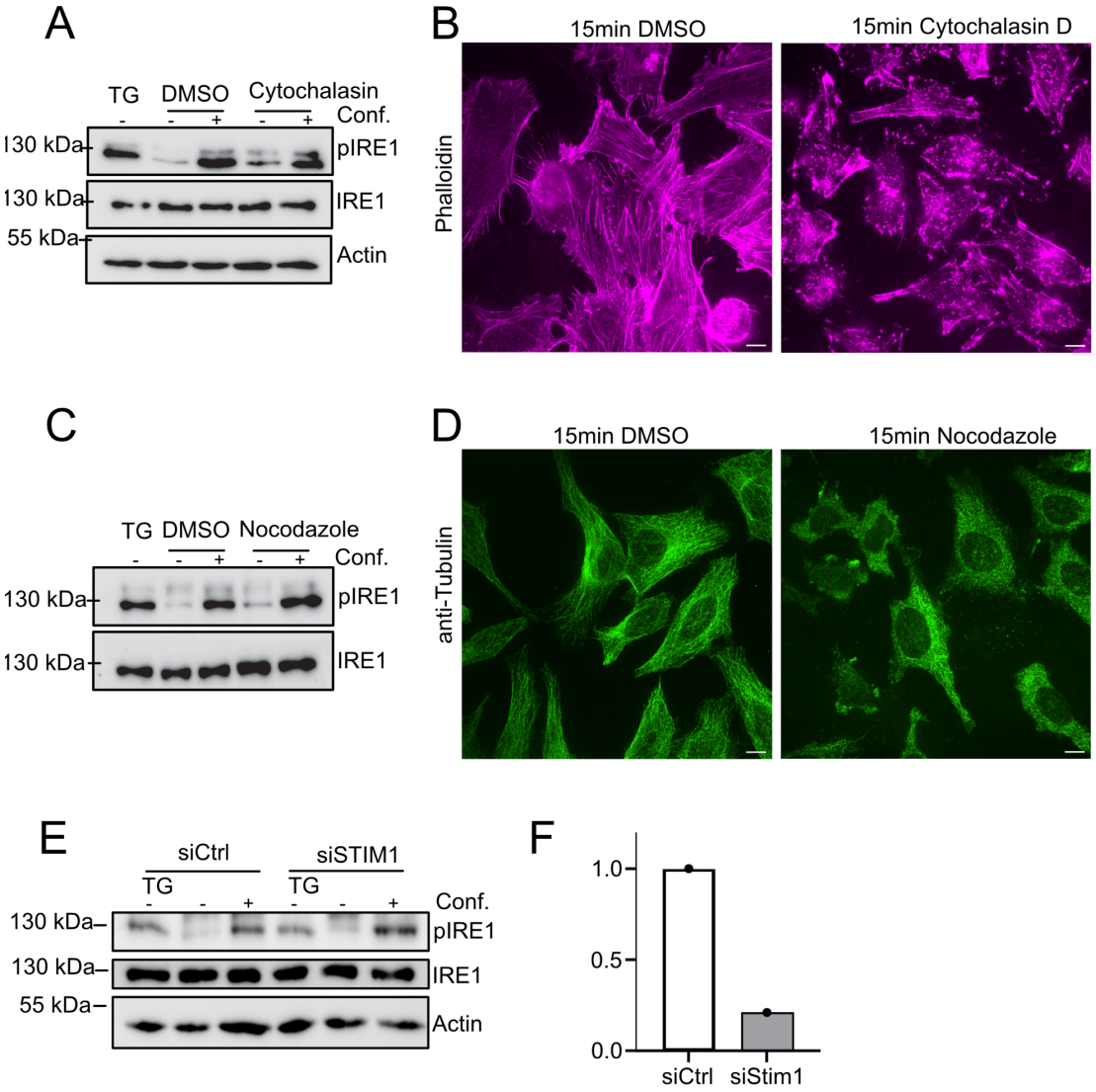

Figure S10. Effect of cytoskeletal disruption on mechano-activation of IRE1. ***A:*** HeLa cells were treated with the actin depolymerization agent Cytochalasin D (500 nM, 15 min pre-incubation before confinement). Cells were either not confined (-) or confined to 3 µm (+) for 30 min followed by lysis and immunoblotting as indicated. ***B:*** Representative cells showing disassembly of the actin cytoskeleton following cytochalasin treatment. Actin was stained using fluorescent phalloidin. ***C:*** HeLa cells were treated with the microtubule depolymerization agent nocodazole (2 µM, 15 min pre-incubation). Cells were either not confined (-) or confined to 3 µm (+) for 30 min followed by lysis and immunoblotting as indicated. ***D:*** Representative cells showing disassembly of the microtubule network following nocodazole treatment. Microtubules are visualized by immunofluorescence staining against tubulin. TG indicates treatment with thapsigargin (3 µM, 1 h). Immunoblot in panel A is representative of 4 independent experiments. Immunoblot in panel B is representative of 3 independent experiments. ***E:*** HeLa cells were treated with non-targeting siRNA (siCtrl) or siRNA targeting STIM1 (siSTIM1) for 72 h before being exposed to either no treatment (-), 3 µM of thapsigargin for 1 h (TG) or confinement to 3 µm for 30min (+), followed by lysis and immunoblotting as indicated. ***F:*** Efficiency of siRNA mediated depletion of STIM1. HeLa cells were treated with either non-targeting siRNA (siCtrl) or siRNA targeting STIM1 (siSTIM1) for 72 h before lysis and quantitative RT-PCR for STIM1 mRNA. Quantifications of all immunoblots are available in supplementary Table S2.

Figure S11

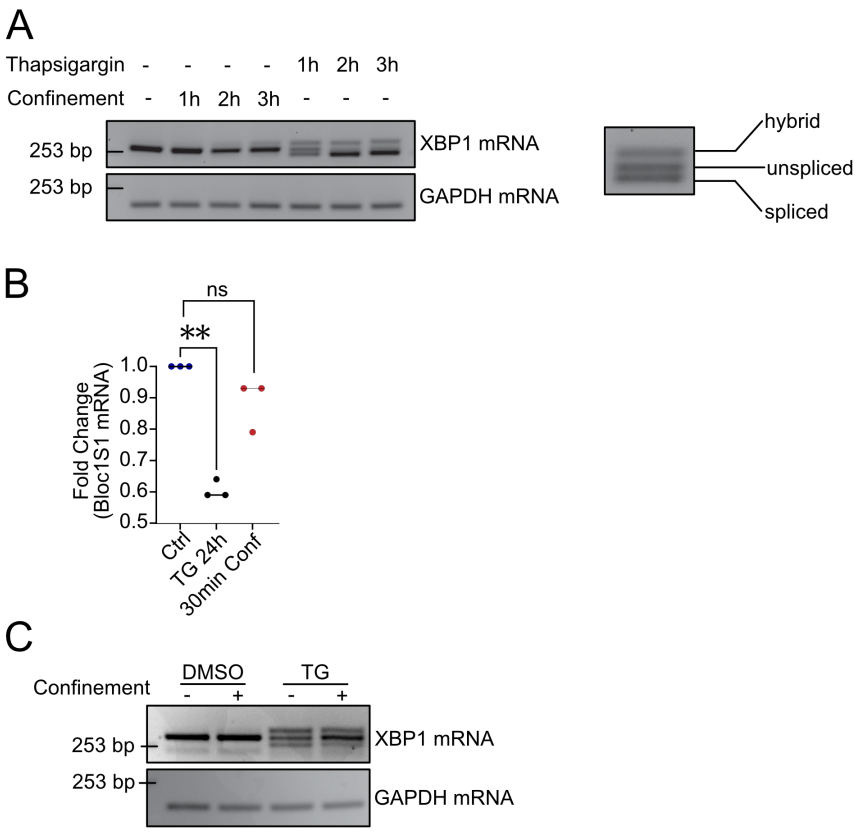

Figure S11. ***A:*** HeLa cells were either treated with 3 µM thapsigargin or exposed to 3 µm confinement for 1-3 h, followed by RNA isolation, cDNA synthesis and PCR amplification of total XBP1 and GAPDH using specific primers. PCR products were resolved on a 3% agarose gel as indicated. On the right side, the 1h thapsigargin-treated condition was magnified and the identity of the unspliced, spliced and hybrid band of XBP1 is labelled to facilitate the interpretation of the experiment. ***B:*** qPCR assay testing for RIDD activity on Bloc1S1 mRNA. HeLa cells were either treated with thapsigargin (3 µM, 24 h) or confined to 3 µm for 30 min. RNA was isolated after treatment and Bloc1S1 target sequence amplified in qPCR using specific primers. Results were normalized to GAPDH and fold changes calculated using the 2^-(ΔΔCt) method. p-values were calculated using one sample t-test (ns $p>0.05$, **$p<0.01$).***C:*** HeLa cells were either treated with thapsigargin (TG) or DMSO and either left undisturbed (-) or exposed to 3 µm confinement for 1 h, followed by RNA isolation, cDNA synthesis and PCR amplification of XBP1 and GAPDH using specific primers. PCR products were resolved on a 3% agarose gel as indicated. Quantifications of XBP1 splicing from all agarose gels are available in supplementary Table S2.

Figure S12

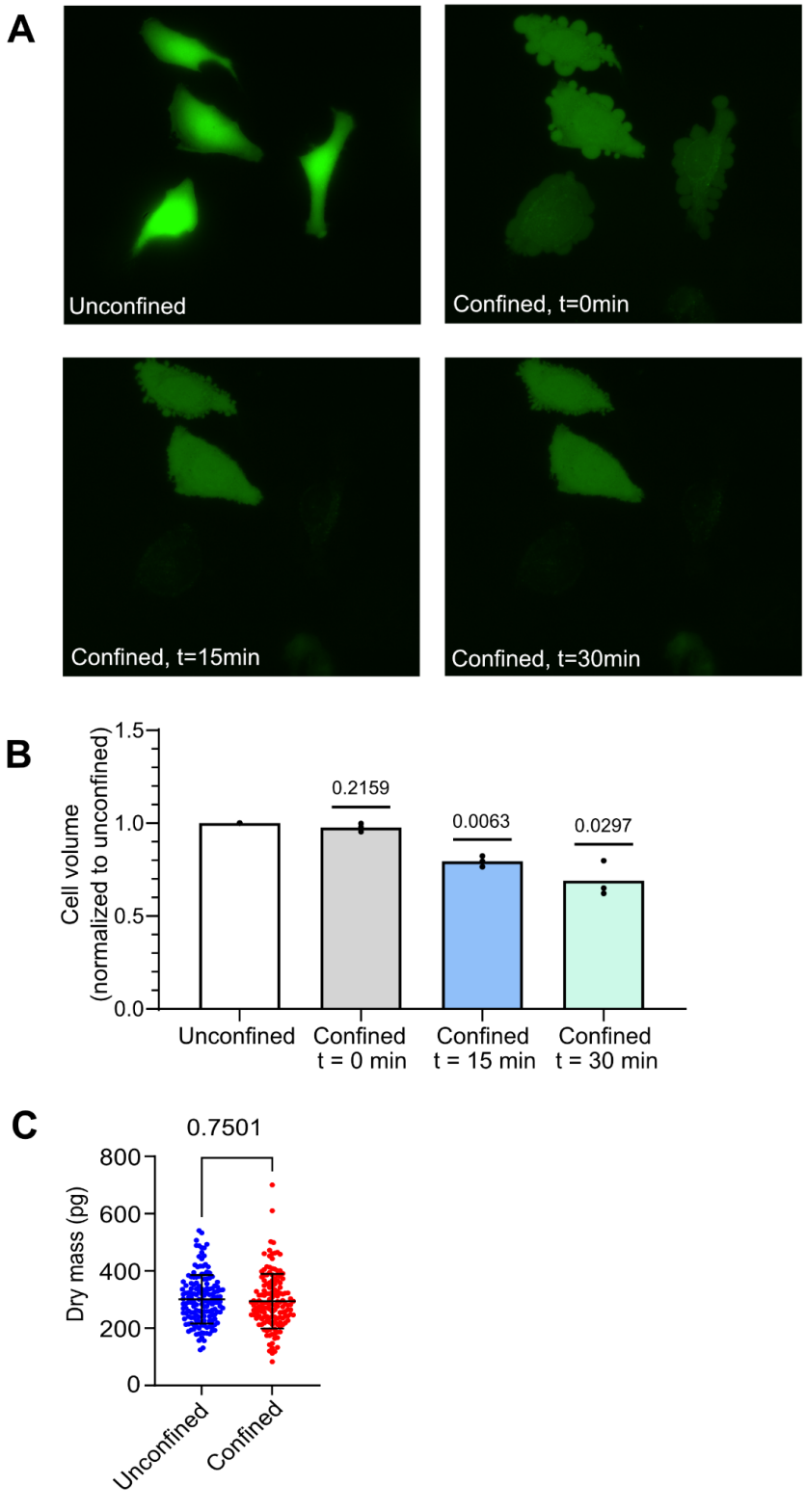

Figure S12. Confinement results in a reduction of cell volume. **A:** Representative images of Calcein-AM widefield live image fluorescence during confinement: Unconfined, immediately after 3 µm confinement (0 min), 15 and 30 min after confinement. **B:** Relative cell volume changes under confinement, normalized by the Unconfined condition. p-values were <calculated using one sample t test, *N*=3. **C:** Dry mass measurements (pg) of control (total 153 cells) and confined cells (total 145), p-values were calculated using one sample t test, N=3.

Figure S13

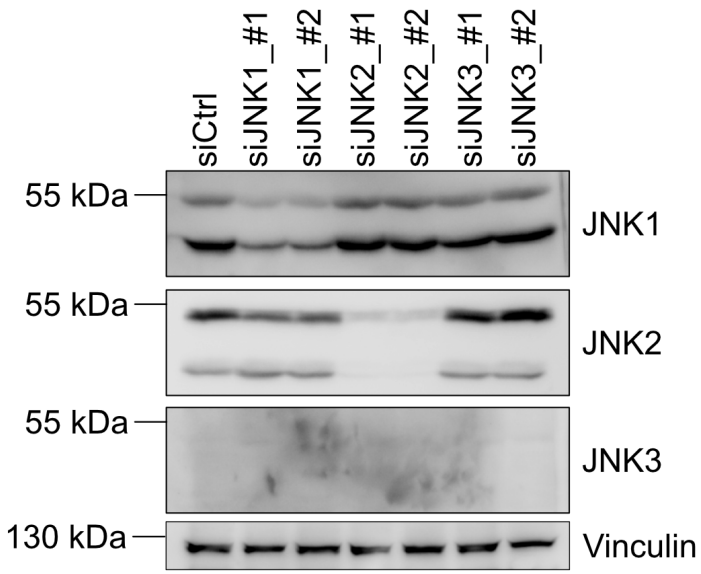

Figure S13. HeLa cells were transfected with two different siRNA for the three isoforms of JNK (JNK1-3). After 48 h, cells were lysed and immunoblotted as indicated. Note that HeLa cells do not express JNK3. Quantifications of all immunoblots are available in supplementary Table S2.

Figure S14

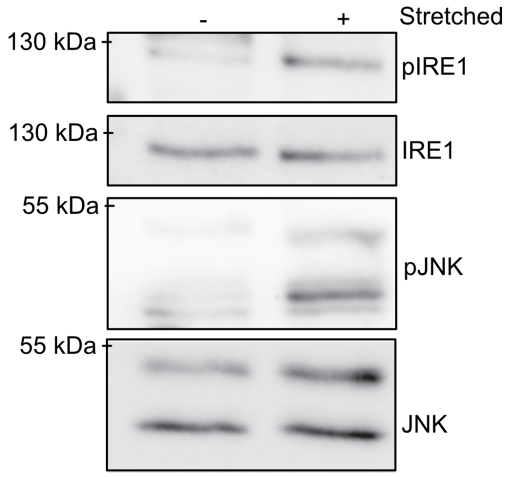

Figure S14. Phosphorylated IRE1 and JNK in passively stretched muscle tissues. Tissues were stretched by 15% of their original length for 30 min followed by lysis and immunoblotting as indicated. Immunoblot is representative of 3 independent experiments. Quantifications of all immunoblots are available in supplementary Table S2.

Supplementary movie S1: Formation of IRE1-GFP clusters under confinement. HeLa cells expressing IRE1-GFP were confined to 3 μm for 1 h and imaged under a spinning disk confocal microscope in a 5 min interval.

Supplementary movie S2: Dissolving of IRE1-GFP clusters after confinement. HeLa cells expressing IRE1-GFP were confined to 3 μm for 1 h. After removing confinement, cells were imaged under a spinning disk confocal microscope in a 5 min interval for 1 h.

Supplementary Material: Mathematical model of diffusion-limited IRE1 clustering

Here we describe a mathematical model to estimate the timescale of IRE1 aggregation on the ER membrane after the application of mechanical loading (membrane tension). We model the system as N IRE1α molecules diffusing on an ER membrane of area A. Without the application of tension, the IRE1α molecules are assumed to be uniformly dispersed across the membrane as monomers[1]. Upon application of membrane tension, a short-ranged membrane-mediated attractive force arises between the monomers leading to aggregation. As observed experimentally, once clusters grow past a certain size M_c, they become immobile, only growing by adsorbing smaller still-mobile clusters. Using Smoluchowski's coagulation equation, we calculate the evolution of the mean cluster size, $\langle s \rangle(t)$, following application of the tension.

Using biologically motivated values for parameters, the model predicts the timescale for IRE1 cluster formation is $\tau_{1/2} = 373$ s. Hence, the model estimates that full clustering of IRE1α should occur several minutes following the application of a tensile stress to the ER membrane. This would be a lower bound on IREα phosphorylation since the time required for force transmission to the ER and autophosphoylation once clusters have formed are not accounted for.

Model Details

Consider a membrane patch with area A containing N IRE1 monomers. Without application of membrane tension, the molecules are assumed to interact very weakly so that the proteins are uniformly distributed across the membrane with density $\rho = N/A$. At time zero, a tension is applied to the membrane, which creates a membrane-mediated attractive potential, $U(r)$, between IRE1 molecules. This potential drives IRE1 to aggregate into clusters.

The cluster formation dynamics can be described by the Smoluchowski coagualtion equation (Smoluchowski 1916)

$$\frac{dn_s}{dt} = \frac{1}{2}\sum_{\substack{i+j=s \\ i,j>1}} K_{ij}\, n_i n_j - n_s \sum_{j=1}^{\infty} K_{sj}\, n_j, \quad s = 1,2,3,\ldots \tag{S1}$$

where n_s is the number of clusters of size s and K_{ij} is the coagulation kernel that gives the rate at which clusters of size i and j combine to form cluster of size $i + j$. Solving equation (S1) with initial condition $n_1(0) = \rho$ and $n_s(0) = 0$ for $s > 1$ gives the cluster size distribution as function of time. Since the total protein density is conserved,

[1] (Belyy et al. 2022) found that, at endogenous levels of expression, IRE1α is primarily dimeric in the unstressed state, forming small oligomers upon chemical stress induction. If we instead assume a dimeric initial population, the model would remain the same except with $N \to N/2$, which would double $\tau_{1/2}$ and τ_M.

$$\sum_{s=1}^{\infty} s\, n_s(t) = \rho, \tag{S2}$$

the mean cluster size is given by

$$\langle s \rangle(t) = \frac{\rho}{\sum_s n_s\,(t)} = \frac{\rho}{n_{total}(t)}. \tag{S3}$$

The dynamics of the cluster size distribution is governed by the coagulation kernel. We next describe the calculation of K_{ij} for IRE1 on the ER membrane.

Coagulation Kernel

Since the copy number of IRE1 in cells is relatively low and the ER membrane area is large, we consider aggregation dynamics in the dilute limit. As such, we will first consider the dynamics of a pair of IRE1 clusters containing i and j monomers, respectively. The probability density, $P_{ij}(r,t)$, of an i −mer and j −mer being a distance r apart at time t is governed by the Smoluchowski equation

$$\frac{\partial P_{ij}}{\partial t} = D_{\text{rel}} \nabla \cdot \left[\nabla P_{ij} + \beta P_{ij} \nabla U_{ij}(r)\right], \tag{S4}$$

where $D_{\text{rel}} = D_i + D_j$ is the relative diffusion coefficient with D_i being the diffusion coefficient of a cluster of size i in the ER membrane. $U_{ij}(r)$ is the effective potential between clusters of sizes i and j and $\beta = k_B T$. Equation (S4) captures the competition between diffusive spreading and the tendency to cluster due to the membrane-mediated attractive force.

Next, we assume that the coagulation of clusters of size i and j into a single cluster of size $i + j$ is encounter-limited and occurs when they are separated by a capture radius $b_{ij} = a(\sqrt{i} + \sqrt{j})$, where a is the capture radius of IRE1 monomers. Under these conditions, the coagulation kernel is given by the long-time limit of the 2D encounter rate

$$K_{ij} = k_{ij}^{2D} = \frac{2\pi\left(D_i + D_j\right)}{\mathcal{I}}, \quad \mathcal{I} = \int_{b_{ij}}^{R(t)} \frac{e^{\beta U_{ij}(r)}}{r} dr. \tag{S5}$$

For a system of finite density, $R(t)$ is the Weigler-Seitz cell size (Wigner and Seitz 1933), which it the effective circular patch occupied by each protein or protein cluster and is initially given by $R = \sqrt{\pi\rho}$. As proteins form clusters, the space between the clusters will increase, making R time dependent and given by $R(t) = \sqrt{\pi n_{total}(t)}$, where $n_{total}(t)$ is the total number of clusters of all sizes.

In general, the diffusion coefficients will depend on cluster size. For proteins (or protein clusters) diffusing in a 2D membrane, the diffusion coefficient of a cluster of size s is given by the Saffman-Delbrück equation (Saffman and Delbrück 1975)

$$D^{SD}(s) = \frac{k_B T}{4\pi\eta_m}\left[\ln\left(\frac{l_{SD}}{b(s)}\right) - \gamma_E\right], \tag{S6}$$

where η_m is the membrane viscosity, and $l_{SD} = \eta_m/\eta_s$ is the ratio of membrane viscosity to the viscosity of the surrounding medium and provides a characteristic length scale for the diffusion, and $\gamma_E = 0.577$ is the Euler-Mascheroni constant. Here, we take $l_{SD} = 1\ \mu$m. If we

assume the clusters are circular, then the cluster size $b(s) = \sigma\sqrt{s}$. Equation (S6) can be rearranged in terms of the diffusion coefficient for a monomer as

$$D^{SD}(s) = D_1\left(1 - \frac{\ln(s)}{2\Lambda}\right), \quad \Lambda = \ln\left(\frac{l_{SD}}{b(1)}\right) - \gamma_E. \tag{S7}$$

The logarithmic scaling of D^{SD} with cluster size means that the diffusion coefficient changes only slightly for large clusters. For example, $D^{SD}(100) \approx 0.59D_1$. However, IRE1 foci in the ER are observed to be approximately immobile (Li et al. 2010). This is likely due to diffusive trapping of large aggregates by the ER morphology, or cytoskeletal interactions that immobilize larger clusters. The transition from mobile to immobile clusters occurs for oligomers between 10-100 molecules (Li et al. 2010). To include this effect, we introduce a mobility cutoff for clusters with size $s > M_c$ such that the diffusion coefficient for a cluster of size s is

$$D(s) = \begin{cases} D^{SD}(s), & \text{if} \quad s < M_c \\ 0 & \text{otherwise.} \end{cases} \tag{S8}$$

Lastly, to compute K_{ij} we must also specify an interaction potential between clusters $U_{ij}(r)$. While data constraining such a potential for IRE1 clusters of different sizes does not, to our knowledge, exist, we can constrain the function on physical grounds and based on previous simulation results for monomer-monomer interactions (Hossain and Stroberg 2024). We will also make the assumption that the potential of mean force is the same for interactions between all cluster sizes such that $U_{ij}(r) = U(r)$. Molecular dynamics calculations of the potential of mean force for IRE1 monomers indicate that the membrane-mediated attraction is relatively short ranges ($\sim$ 4 nm) with an energy well depth many times $k_\mathrm{B}T$. Hence, we assume that the potential is radially symmetric and takes the form of a 9-3 Lennard-Jones potential

$$U(r) = \frac{\varepsilon}{2}\left[\left(\frac{\sigma}{r}\right)^9 - 3\left(\frac{\sigma}{r}\right)^3\right], \tag{S9}$$

where ε determines the energy well depth of the interaction and σ determines the interaction range such that $U(\sigma) = -\varepsilon$ is the minimum potential energy. By separating the integral $\mathcal{I}$ into three regions, we can see that the coagulation kernel is relatively insensitive to the parameters ε and σ. Substituting $x = r/\sigma$ gives,

$$\mathcal{I} = \int_1^{\frac{R}{\sigma}} \frac{e^{0.5\beta\varepsilon\left(x^{-9} - 3x^{-3}\right)}}{x}\, dx. \tag{S10}$$

The potential is effectively zero beyond $r = 10\sigma$, at which point the proteins and protein clusters are essentially freely diffusing. Hence, we divide the integral into two sections

$$\mathcal{I} \approx \mathcal{I}_1 + \mathcal{I}_2 = \int_1^{10} \frac{e^{0.5\beta\varepsilon\left(x^{-9} - 3x^{-3}\right)} - 1}{x}\, dx + \int_1^{\frac{R}{\sigma}} \frac{1}{x}\, dx, \tag{S11}$$

where the first integral captures the effect of the potential well on the encounter rate and is always negative, and the second integral is the free-diffusion approximation, which evaluates to

$$\mathcal{I}_2 = \ln\left(\frac{R}{\sigma}\right). \tag{S12}$$

For $\varepsilon = 10k_\mathrm{B}T$, $\mathcal{I}_1 \approx -1.09$, and is only weakly sensitive to changes in ε (e.g, for $\mathcal{I}_1(\varepsilon = 5\ k_\mathrm{B}T) \approx -0.86$ and $\mathcal{I}_1(\varepsilon = 20\ k_\mathrm{B}T) \approx -1.32$). $\mathcal{I}_2$ will be smallest for the initial state of fully

monomeric IRE1, for which $R(0) = \sqrt{\pi\rho} \approx 1.58\mu$m. Hence, using $\sigma = 1.2$ nm, $\mathcal{I}_2 \geq \ln(1367) = 7.18$ for all times. As clusters form, $\mathcal{I}_1$ remains constant while $\mathcal{I}_2$ grows with increasing R. Hence, we assume $\varepsilon = 10\ k_{\mathrm{B}}T$, noting that the encounter rate and coagulation kernel are relatively insensitive to this choice.

Model Parameters

To calculate clustering dynamics for IRE1 in cells, we need the diffusion coefficient and density of IRE1 in the ER membrane, the effective capture radius, and the strength and length-scale of the protein-protein potential of mean force. These parameters, and descriptions of how they were estimated, are given in Supplementary Table *1*.

Parameter	Description	Value	Source
D	IRE1α diffusion constant	0.18 μm^2/s	(Belyy et al. 2022)[2]
N	cellular IRE1α copy number	8.4×10^3 molecules	(Cho et al. 2022)[3]
A	Area model ER membrane	2×10^4 μm^2	(Belyy et al. 2020)[4]
ε	Potential depth	10 k_BT	-[5]
σ	Potential length scale	1.2 nm	(Hossain and Stroberg 2024)[6]
M_c	Mobility cutoff size	25 molecules	(Li et al. 2010)[7]
a	Monomer capture radius	σ nm	-

Supplementary Table 1. Model Parameters.

Calculation of Clustering Time

Using the parameters from Supplementary Table *1*, the cluster size distribution as a function of time can be calculated by integrating Equation (S1) numerically. The timescale of aggregation, $\tau_{1/2}$, is calculated as the time at which the mean cluster size equals the mobility cutoff size, M_c. The clustering dynamics and the clustering time are shown in Figure 3F of the main text. Below we provide an analytical approximation for this timescale assuming a constant aggregation kernel.

Constant-kernel approximation

Initially, the system is fully monomeric so the aggregation dynamics is dominated by the monomer-monomer reaction rate, K_{11}. Using this observation along with the method of moments, we can estimate the timescale for IRE1 clustering analytically. In general, K_{11} will

[2] Determined for Halo-tagged IRE1α in endogenous mix of monomers and dimers.

[3] Estimated from whole-cell mass spectrometry of HEK293T cells.

[4] Taken to twice the estimated area of the ER membrane in U2-OS cells.

[5] See above discussion on the sensitivity of the model to this parameter.

[6] Estimated as the location of the minimum of potential of mean force between yeast Ire1 monomers under 5 pN/nm applied tension.

[7] Immobile foci are estimated to be between 10-100 monomers based on fluorescence intensity.

depend on the distribution of cluster sizes, requiring a closure model. Here, since the number of monomers is relatively large, we expect the initial rate, $K_{11}(n_T = \rho) = \bar{K}$, to provide a reasonable approximation to the early-time cluster dynamics. By summing over the cluster size distribution and assuming a constant kernel, Equation (S1) yields an equation for the total number of clusters

$$\frac{dn_T}{dt} = \sum_{s=1}^{\infty} \frac{dn_s}{dt} = \frac{K_{11}}{2} n_T^2 - K_{11} n_T^2 = -\frac{K_{11}}{2} n_T^2. \tag{S13}$$

The constant-kernel assumption leads to an upper-bound on the coagulation rate, and hence a lower-bound on the the coagulation timescale since the kernel will decrease as the number of individual clusters decreases. Equation (S13) integrates to

$$n_T(t) = \frac{n_T(0)}{1 + \frac{t}{\tau_0}}, \quad \tau_0 = \frac{2}{\bar{K} n_T(0)}. \tag{S14}$$

Substituting into Equation (S3) and noting the $n_T(0) = \rho$, gives

$$\langle s \rangle(t) = 1 + \frac{t}{\tau_0}. \tag{S15}$$

τ_0 is approximately the time for the monomers to have formed dimers. We can estimate the time for clusters of size M_c to form as

$$\tau_{M_c} = M_c \tau_0 = \frac{2M_c}{\bar{K}\rho}. \tag{S16}$$

This linear approximation underestimates the timescale, but is a good approximation when the dynamics is primarily governed by monomer binding. If the pool of monomers is large compared to M_c, this will provide a reasonable approximation to the timescale over which immobile IRE1 foci form. For the parameters given in Supplementary Table *1*, $\tau_{M_c} = 289\ s$, which is within 23% of the estimated timescale from solving the full Smoluchowski equation, suggesting the coagulation of larger clusters plays a small, but non-negligible role in IRE1 foci formation.

References

Belyy, Vladislav, Ngoc Han Tran, and Peter Walter. 2020. "Quantitative Microscopy Reveals Dynamics and Fate of Clustered IRE1α." *Proceedings of the National Academy of Sciences of the United States of America* 117 (3): 1533–42. https://doi.org/10.1073/pnas.1915311117.

Belyy, Vladislav, Iratxe Zuazo-Gaztelu, Andrew Alamban, Avi Ashkenazi, and Peter Walter. 2022. "Endoplasmic Reticulum Stress Activates Human IRE1α through Reversible Assembly of Inactive Dimers into Small Oligomers." *eLife* 11 (June): e74342. https://doi.org/10.7554/eLife.74342.

Cho, Nathan H., Keith C. Cheveralls, Andreas-David Brunner, et al. 2022. "OpenCell: Endogenous Tagging for the Cartography of Human Cellular Organization." *Science* 375 (6585): eabi6983.

Hossain, Md Zobayer, and Wylie Stroberg. 2024. “Bilayer Tension-Induced Clustering of the UPR Sensor IRE1.” *Biochimica et Biophysica Acta (BBA) - Biomembranes* 1866 (2): 184262. https://doi.org/10.1016/j.bbamem.2023.184262.

Li, Han, Alexei V. Korennykh, Shannon L. Behrman, and Peter Walter. 2010. “Mammalian Endoplasmic Reticulum Stress Sensor IRE1 Signals by Dynamic Clustering.” *Proc Natl Acad Sci U S A* 107 (37): 16113–18. https://doi.org/10.1073/pnas.1010580107.

Saffman, P. G., and M. Delbrück. 1975. “Brownian Motion in Biological Membranes.” *Proceedings of the National Academy of Sciences* 72 (8): 3111–13. https://doi.org/10.1073/pnas.72.8.3111.

Smoluchowski, M. V. 1916. “Drei Vortrage Uber Diffusion, Brownsche Bewegung Und Koagulation von Kolloidteilchen.” *Zeitschrift Fur Physik* 17 (January): 557–85.

Wigner, E., and F. Seitz. 1933. “On the Constitution of Metallic Sodium.” *Physical Review* 43 (10): 804–10. https://doi.org/10.1103/PhysRev.43.804.